Algerian Journal of Electrical Systems and Sustainability (AJESS)

ISSN **3088-7992**, E-ISSN **3088-800X**.
Vol:2, No:1, pp.1-19 (2026)
https://univ-bejaia.dz/revue/AJESS

Received: 17/06/2026 Accepted: 21/06/2026 Published: 30/06/2026

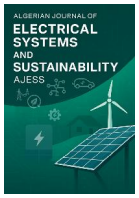

Hybrid AC/DC Power System Stability: An Attempt of Global Approach

Gianni BAKHOS[1], Seddik BACHA[1,2,5], Luigi VANFRETTI[1,3], Juan-Carlos GONZALEZ-TORRES[1], Abdelkrim BENCHAIB[1,4], Jing DAI[1,6,7], Kosei SHINODA[1]

[1] *"SuperGrid Institute SAS, 23 rue de Cyprian, Villeurbanne 69100, France"*
[2] *"Université Grenoble Alpes, CNRS, Grenoble INP, G2ELab, 21 Avenue des Martyrs, Grenoble 38000, France"*
[3] *"Rensselaer Polytechnic Institute, 110 8th Street, Troy, New York 12180, the United States of America"*
[4] *"Conservatoire National des Arts et Métiers, 292 rue Saint Martin, Paris 75003, France"*
[5] *"Université de Guyane, Espace-Dev, UMR 228, Cayenne, F-97300, France"*
[6] *"Sorbonne Université, CNRS, Laboratoire de Génie Electrique et Electronique de Paris, Paris 75252, France"*
[7] *"Université Paris-Saclay, Ecole CentraleSupélec, Laboratoire de Génie Electrique et Electronique de Paris, Gif-sur-Yvette 91192, France"*

Corresponding author: seddik.bacha@univ-guyane.fr

Abstract

In this paper, a new control coordination strategy is proposed to address multiple stability problems that may arise in HVAC/HVDC power systems. The stability issues studied in this paper include small-signal, rotor angle, frequency, and DC voltage. A benchmark composed of two 2-area AC systems inspired by Kundur system connected through a Modular Multilevel Converter-based (MMC) multi-terminal DC (MTDC) system is proposed to study multiple stability issues. To enhance the global security of the considered benchmark power system, supplementary power converter controllers are designed and implemented as ancillary HVDC services. The combination of these services may not always result in satisfactory dynamic performance due to system constraints and control interactions. Therefore, a coordinated strategy is proposed and evaluated through a comparative study. The advantages of this method are mainly: 1) AC & DC stability phenomena – usually studied separately – are considered and enhanced in a global approach, simultaneously, and 2) the coordination strategy guarantees minimal control interactions during operation without the need of modifying the tuning of the controller parameters.

Key words: AC/DC Power System; Stability Control; HVDC; MMC; Benchmarking; MTDC

1. Introduction

With the development of high-voltage direct current (HVDC) grids, hybrid AC & DC power systems have been established, giving rise to new power stability challenges. Conventionally, most of the power sources are synchronous machines. Some of them are equipped with a power system stabilizer (PSS) to damp the oscillations, and some may contribute to AC voltage and frequency regulation. With the increase of power production from electronic-interfaced renewable energy sources, the share of synchronous machines within the power system is being reduced. Therefore, the contributions of the remaining ones to power system stability become less and less significant. Concurrently, more AC/DC power conversion stations interface the conventional AC power system and DC system. Consequently, long-distance HVDC power transmission is developed and new opportunities to use AC/DC stations to contribute to the stability of the AC grid appear [1]. However, it should be noted that depending on the control mode (grid-following or grid-forming mode, with or without synthetic inertia, capable or not of exchanging power in case of a fault (fault ride-through capability), etc.), power converters behave differently. The behavior of the power converters is determinant of the stability of the AC system to which they are connected. This paper focuses on active power exchange between the converters and the AC system. The fluctuation of active power impacts DC and AC grids, which may jeopardize the grids stability. The stability aspects that this paper deals with are small-signal (related to inter-area power oscillations), transient and steady-state (frequency, DC voltage and rotor angle). In the following, the stability aspects mentioned before are assessed through indicators and enhanced through HVDC control strategies.

Classical approaches that aim to enhance AC grid's stability using HVDC grids rarely combine different aspects of system's stability in a global approach. The idea of combining controllers was proposed in [2] as one of the existing possibilities to enhance AC&DC stability. In [3]–[8], small-signal stability was studied in isolation, while in [9]–[15] the frequency support was examined. In [16]–[21] DC voltage controls (mostly droop-based) were studied, and [22]–[26] examine the rotor angle stability. The interaction between DC voltage and frequency support

was evaluated in [14], [17] and control methods to limit these interactions were also proposed. However, the studies do not consider the interactions with other control loops from a global power system perspective.
The key idea in this work is to propose a new holistic approach to enhance the stability of the power system by coordinating the ancillary services of the HVDC acting on active power. To present this new idea, a benchmark system composed of two-are four-generator power systems (inspired by 'Kundur' test system models) connected through a four-terminal meshed MMC-based MTDC system is proposed (**Erreur ! Source du renvoi introuvable.**). A preliminary examination of the implemented controllers is conducted before combining them and then proposing a coordination strategy.
The remainder of the paper is organized as follows. In Section **Erreur ! Source du renvoi introuvable.**, we describe the HVDC ancillary services and study the impact of each one individually. In Section 0, a comparative study is made on the proposed benchmark. In the case studies, three ancillary services are implemented incrementally. The coordination strategy between them is explained also in this Section 0, and concluding remarks are presented in Section 0.

Nomenclature

AC	alternating current
ADC	angle difference controller
DC	direct current
FCR	frequency containment reserve
HVAC	high-voltage AC
HVDC	high-voltage DC
MMC	modular multi-level converter
MTDC	multi-terminal HVDC
PCC	point of common coupling
POD	power oscillation damping
PSS	power system stabilizer
TSO	transmission system operator
V_{dc}	DC voltage
VSC	voltage source converter

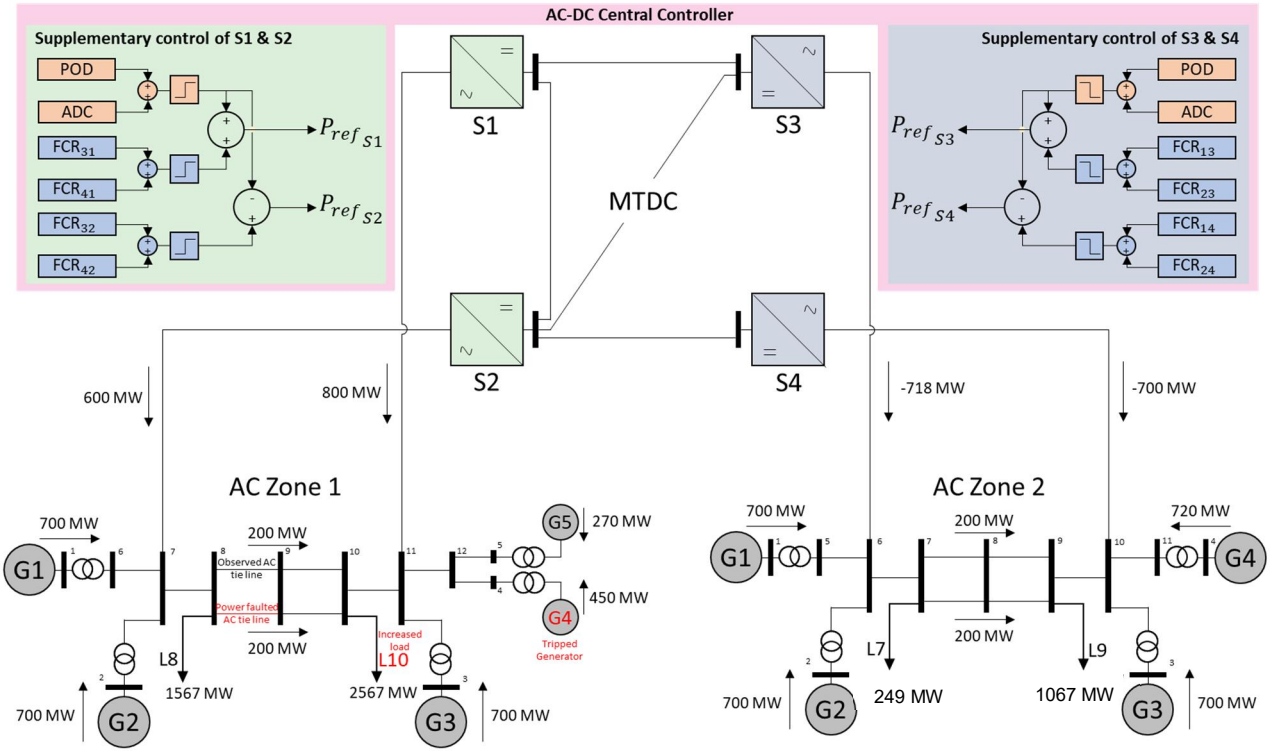

Fig. 1. Benchmark for the comparative study. Initial active power flow and implemented HVDC controllers are indicated on the figure.

2. HVDC ancillary services and their realization

2.1. Power system dynamics

For a system composed of N synchronous machines connected to the same synchronous area, the modified swing e

δi=ωiMiω̇i= −Diωi+Pm,i−Pe,i
(1)**Erreur ! Source du renvoi introuvable.** of the ith synchronous machine $\forall i \in \{1,..,N\}$ are:

$$\begin{aligned} \dot{\delta}_i &= \omega_i \\ M_i\dot{\omega}_i &= -D_i\omega_i + P_{m,i} - P_{e,i} \end{aligned} \quad (1)$$

where δ_i is the rotor angle, ω_i the rotor speed deviation from the speed corresponding to the nominal frequency (synchronous speed), M_i is the inertia coefficient, D_i is the damping torque inherent to the machine, $P_{m,i}$ is the mechanical power given by the controlled turbine, $P_{e,i}$ is the electrical output power of the machine.

These equations govern the dynamics of AC power system. When AC/DC power converters interface AC and HVDC systems, the power exchange $P_{HVDC,k}$ between a converter k and a bus B_{ij} in a synchronous zone l modifies the classical AC dynamics. The convention in this paper considers power flow positive from DC to AC side (i.e., $P_{HVDC,k} > 0$ when converter extracts power from DC and injects it in AC).

Based on the AC and DC dynamics, the power references of the AC/DC converters are modified by the implemented controllers (regulating the AC frequency, rotor angle, power oscillations and DC voltage). A focus on the potential supplementary controls is made in the next part.

2.2. Selected services

The expected HVDC functionalities [27] that this paper tackles are:

- AC line emulation, called in this paper Angle Difference Control (ADC)
- Power oscillation damping (POD)
- Frequency support (FCR)

These stability enhancement strategies offered by ancillary services are valid if DC voltage is not at risk since this risk can lead to HVDC system loss, and no ancillary service could be provided anymore. If an event puts DC voltage at risk, the mentioned ancillary services should be stopped until the DC voltage stability becomes guaranteed again.

In the proposed benchmark (see Fig. 1), the following is valid:

The initial AC active power flow is indicated in the figure.

Converters' rated values are: $\{V_{dc} = 640 \text{ kV}; P = 1 \text{ GW}\}$.

The converters are all operating in DC voltage droop mode with same droop gain $K_{V_{dc}} = 8$ MW/kV, such that:

$$P^*_{DC_{droop_k}}(t) = K_{V_{dc}} \cdot \left(V^k_{dc}(t) - V^k_{dc_0}(t)\right) \quad (2)$$

The simulations have been developed using the Dymola software based on Modelica language. The works use the Open IPSL library [28] and HVDC Library developed at SuperGrid Institute [29]–[31]. The initialization of the AC zones has been done through Grid Cal tool [32].

2.2.1. AC Line Emulation – Angle Difference Control (ADC)

Based on phase angles' difference at the PCCs of the AC/DC stations, the ADC sends a power reference to the converters involved in extracting power at one PCC, transfers it through a DC path and injects it at another converter embedded in the same AC synchronous zone. The main purpose of this service is to reinforce rotor angle stability of an AC system by emulating the behavior of AC lines for power transmission. It is normally used for steady-state rotor angle enhancement: it reduces the angle difference between the PCCs which lowers the amount of power transmitted through the AC lines parallel to the DC path. This reduces the risk of AC overcurrent and system split. As it is based on angle measurements, AC line emulation cannot be applied to two non-synchronous power systems. Besides, this service needs well-established communication between the converters used so that the same power is exchanged between the two converters.

For a couple of converters k and j connected to the same synchronous area, ADC control sends the following power references [33]:

$$\begin{aligned} P^*_{ADC\,kj}(t) &= K_{ADC,kj} \cdot \left(\theta_j(t) - \theta_k(t)\right) && (3.a) \\ P^*_{ADC\,jk}(t) &= -P^*_{ADC\,kj}(t) && (3.b) \end{aligned} \quad (3)$$

where $\boldsymbol{K_{ADC,kj} > 0}$ is the gain of the ADC between converters $\boldsymbol{k}$ and $\boldsymbol{j}$, $\boldsymbol{\theta_k}$ and $\boldsymbol{\theta_j}$ are the bus angles at the PCCs, and $\boldsymbol{P^*_{ADC_{kj}}}$ is the power reference sent to converter $\boldsymbol{k}$ due to the existing ADC control between it and converter $\boldsymbol{j}$.

The

$P*ADCkjt=KADC,kj\cdot\theta jt-\theta kt$ (3.a) $PADC*jkt=-PADC*kjt$ (3.b)

(3.b) ensures that power balance is respected so that DC voltage remains stable.

A

l

o

w

-

p

a

s

s

f

i

l

t

e

r

To understand the impact of the ADC, the controller was solely implemented on the study benchmark. The case study is summarized in **Erreur ! Source du renvoi introuvable.**. The same gain and time constant are used for the ADCs of $\{S_1 \leftrightarrow S_2\}$ and $\{S_3 \leftrightarrow S_4\}$.

R

E

F

As shown in the Fig. 2, AC line emulation by DC path through ADC reduces the steady-state power transfer on the observed AC tie line[1] (in the proposed benchmark, the AC zone 1 can be considered to have two AC areas (left side and right side) connected through four AC tie lines. The tie-line considered to observe the power flow is mentioned in Fig. 1.). Therefore, the effort of compensating for the loss of the AC tie line is shared between the remaining AC system and the DC system.

R

e

f

Table 1. Case study for ADC (check Fig. 1 to see the location of the fault).

1	Contingency	K_{ADC} (MW / °)	τ_{ADC} (s)
4 0	Power fault at Bus 9 in AC zone 1 (t=1s) leading to the trip (t=1.1s) of one AC tie line	1005	5

5 0

Table 2. Case study for POD.

4	Contingency	K_{POD} (MW / Hz)
2 0 7	Load increase at L10 (300 MW or 8.3% of total nominal power of synchronous machines in AC zone 1, at t=1s) leading to a power imbalance and increasing power flow through AC tie-lines.	2500

\

h

\

*

M

E

R

G

E

F

O

R

M

A

T

$$LPF_{ADC,kj}(s) = \frac{\Delta\theta_{out}}{\Delta\theta_{in}} = \frac{1}{1+\tau_{ADC,kj}s} \quad (4)$$

[1] An AC tie line is an electrical transmission line connecting two sub-zones in a synchronous zone.

$$\square ADC, kj\square(s) = \frac{\Delta\theta_{out}}{\Delta\theta_{in}} = \frac{1}{1+\tau_{ADC,kj}s}$$

(4) is added to the ADC to avoid unnecessary power compensation (oscillating power compensation,

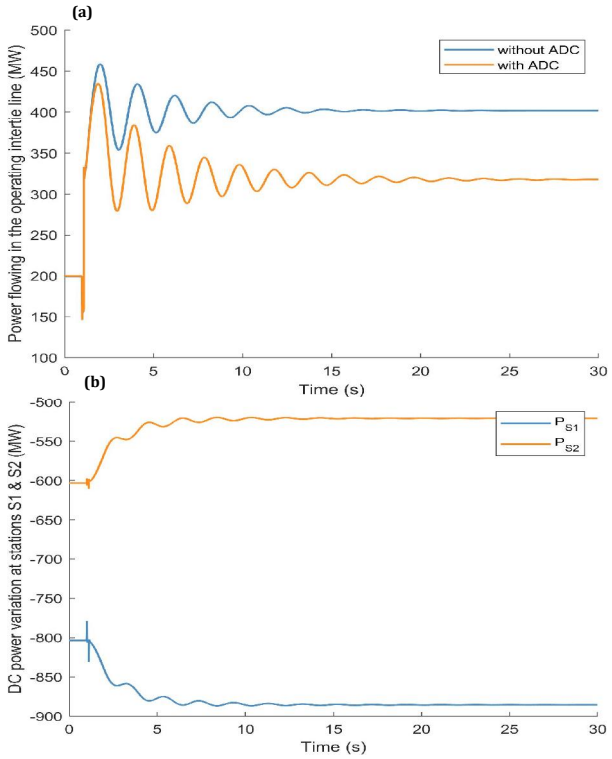

Fig. 2. (a) Active power flowing through the observed AC tie line parallel to the lost line. Steady-state values show ~84 MW less AC power flowing thanks to line emulation by ADC.
(b) DC power flowing at station S1 and S2. The steady-state values show that ~84MW power flows through DC path thanks to the ADC between S1 and S

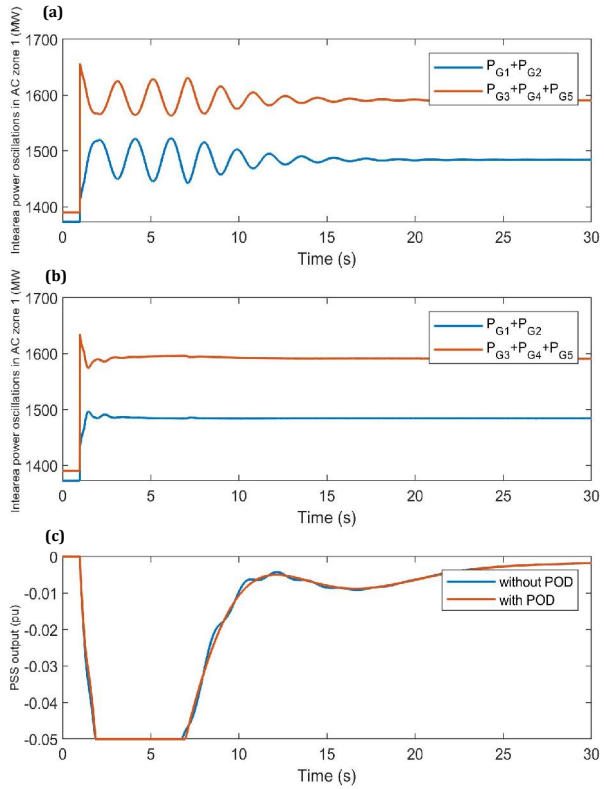

Fig. 3. Power oscillations between left and right areas after contingency in AC zone 1 (without POD (a), with POD (b)). PSS output remains saturated right after contingency in both cases (c).

2.2.2. Power Oscillation Damping (POD)

When an AC synchronous area is subject to power oscillations, an embedded HVDC system can inject damping power in addition to the action of the PSSs by sending opposite power references simultaneously to suitable

converters. Particularly, inter-area power oscillations – which are of electro-mechanical nature – may occur within the same synchronous zone after a disturbance reduces the balancing capability of AC inter-area connections or reduces the damping. The frequency of modes of these oscillations is generally within the range of [0.1; 0.7] Hz [34]. An eigenvalue analysis helps identify the involved inter-area eigenvalues and calculate their frequency and damping ratio. Like for the previous part, this service assumes communication is established between the involved converters.

For a couple of converters k and j connected to the same synchronous area, the POD control sends the following power references:

$$\begin{aligned} P^*_{POD_{kj}}(t) &= K_{POD,kj} \cdot \left(f_j(t) - f_k(t)\right) \\ P^*_{POD_{jk}}(t) &= -P^*_{POD_{kj}}(t) \end{aligned} \quad (5)$$

where $K_{POD,kj} > 0$ is the gain of the POD between converters k and j, f_k and f_j are the measured frequencies at the PCCs, and $P^*_{POD_{kj}}$ is the power reference sent to converter k due to the POD control between it and converter j.

To understand the impact of the POD, the controller was solely implemented on the study benchmark. The same POD gain was chosen for the couples $\{S_1 \leftrightarrow S_2\}$ and $\{S_3 \leftrightarrow S_4\}$. The case study is summarized in **Erreur ! Source du renvoi introuvable.**.

In Fig. 3.a – the case without POD controller – power oscillations appear between {G1, G2} and {G3, G4, G5}. At generator's level, the local frequency (input of the PSS of the generator) decreases sufficiently to saturate the local PSS (Fig. 3.c) which is insufficient to fully damp the inter-area oscillations. In the case with the POD service (Fig. 3.b), although the PSSs remain saturated (Fig. 3.c) due to the local frequency (input of PSS) decrease, the HVDC system helps damp the oscillations by exchanging power between the right and left areas of AC zone 1 t
h
r
2.2.3 Frequency Containment Reserve (FCR)
o The FCR, when activated, implies that a synchronous zone shares the reserve with another synchronous zone t
through HVDC [35].
g The advantage of FCR is to share the disturbance mitigation effort between different AC zones to increase the a
bility of responding to the contingency without losing frequency stability in the disturbed zone. **(a)**

Solutions for frequency support between two synchronous zones are multiple [14]. In this paper, we compare t
two of them.
h
2.2.3.1. Solution based on DC voltage droop control.
e Based on local frequency droop control, converters inject or extract power depending on PCC's frequency deviation from nominal value. The power exchanged between AC and DC systems based on this local control a
ffects the voltage in the DC system which activates DC voltage droop control.
C When this voltage controller is implemented in the same converter used by the frequency droop controller, interactions appear between both controllers [14], [17]. As shown in the mentioned papers, a rescaling of the f
requency control parameters is needed to limit frequency variation.
i However, when DC voltage control is also/only implemented in the converters connected to another s
ynchronous zone, the following happens. The power injected/extracted in the disturbed synchronous zone – due t
o local frequency droop controller – by the converter connected to this zone impacts the DC voltage of the HVDC g
rid. In this case, the stations connected to another synchronous zone and operating in DC voltage control mode react to the voltage perturbation in HVDC grid and extract/inject power from their own synchronous zone. In this process, the power needed in the disturbed AC zone is transferred – through DC voltage droop control – from a
nother AC zone which is considered to propose frequency support to the disturbed AC zone.
h The main drawback of this method is the existing interactions between AC frequency and DC voltage at the i
converting station connected to the disturbed zone [36]. To limit DC voltage variation, enough power reserve s
hould be available for DC droop control, and this may be jeopardized if a converter contributing to DC voltage control trips.
i
2.2.3.2. Solution based on distributed frequency droop control.
s Frequency support can alternatively be based on direct communication means between contributing stations [14] to guarantee power balance in the DC grid and therefore preserve the DC voltage from big variations.
d In this solution, needed power for frequency support is calculated based on local droop controller too but the p
ower references of this controller are directly sent to a couple of converters connected to different synchronous z
ones. For each couple of converters – one connected to the disturbed and the other to an undisturbed synchronous z
one – the power references are sent in opposite signs: if one converter should inject power in an AC zone, the other one from the couple should extract the same amount from the distinct AC zone to which it is connected. T
herefore, power balance is guaranteed within the HVDC grid and DC voltage control reserve is not required.
p
r The FCR power references are determined from:
o
p
o
r
t
i
o

$$P^*_{FCR_{kj}}(t) = K_{FCR,kj} \cdot \left(f_{k,nominal} - f_k(t)\right) - K_{FCR,jk} \cdot \left(f_{j,nominal} - f_j(t)\right)$$
$$P^*_{FCR_{jk}}(t) = -P^*_{FCR_{kj}}(t) \quad (6)$$

where $K_{FCR,kj} > 0$ is the frequency droop gain of the converter k with respect to converter j, $K_{FCR,jk} > 0$ is the frequency droop gain of the converter j with respect to converter k, f_k and f_j are the measured frequencies of these converters, $f_{k,nominal}$ and $f_{j,nominal}$ are the nominal frequencies of the synchronous zones to which converters k and j are connected respectively, and $P^*_{FCR_{kj}}$ is the power reference sent to converter k due to the existing FCR control between it and converter j.

Frequency support can also be provided by stations connected to stored or renewable energy sources, but this is not specifically studied within the scope of this paper.

To determine which synchronous area should contribute to frequency support in priority in real-life operation, TSOs may be based on electricity market prices. This is not within the scope of this technical paper either.

2.2.3.3. Comparison of the two FCR solutions.

In the used benchmark, two solutions of frequency support are tested and compared (Fig. 4).

To understand the impact of the FCR, the controller was solely implemented on the study benchmark. The case study is summarized in Table 3.

Table 3. Case study for FCR

Contingency	Gain of the FCR (MW / Hz)
Load increase at L10 (150 MW or 4.15% of total nominal power in AC zone 1, at t=1s) leading to disequilibrium between production and consumption and heavily loaded AC tie-lines.	750 (only converters connected to AC zone 1 are involved in the FCR service)

After the load increases, the frequency Nadir is the lowest in the case where no frequency support is implemented (Fig. 4.a). Frequency deviation from nominal value (50 Hz) is then enhanced by adding local frequency droop control at the converters S1 and S2. However, with this control, the frequency support interacts with DC droop control and leads to a drop in DC voltage's steady-state (Fig. 4.b). To counteract the interaction with DC voltage control, the solution presented in 0 was tested and the results ('Distributed FCR') show that the FCR's efficiency was increased compared to the 'Local FCR' case. The DC voltage is much less impacted by frequency support as well. In the following, this last FCR solution is used.

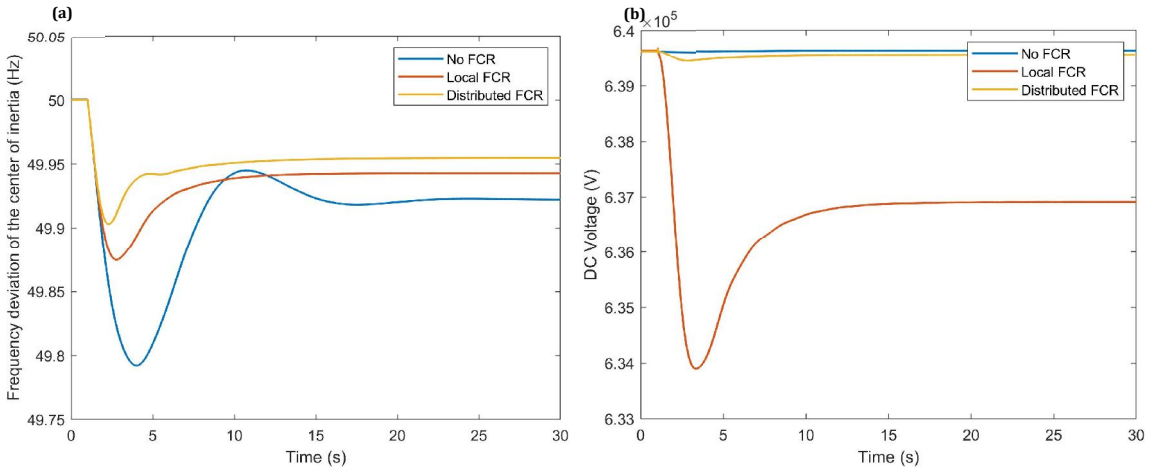

Fig. 4. Frequency deviation to nominal frequency of the center of inertia of disturbed AC zone 1 (a) and DC voltage variation (b) in the cases without FCR, with local droop-based FCR and distributed droop-based FCR.

3. A Comparative Study of Control Designs for Multi-Criteria Stability Enhancement

In the previous section, dedicated control structures were tested for each of the considered stability aspects individually. However, the combination of these controls is not straightforward at least due to the power constraints of the converters. In fact, it is not guaranteed that the direct combination of multiple ancillary services will result in stability enhancement. Instead, it can lead to competition between control outputs leading to antagonist effects (voltage vs frequency control) or cancellation of the control impact (POD vs FCR in case of converter's power saturation).

In most of the literature, the used approaches aim to design the control of one or two [2], [19], [37], [38] of the mentioned stability aspects. In this article, we propose a global approach to enhance the stabilities through a logical combination of the needed controllers.

Therefore, in this part, different strategies of control are evaluated. In the studies, we explore the degrees of freedom offered by the control of MTDC system which is, from AC-DC perspective, constrained by the converters' power rating and their ability to inject/extract power (AC side saturation, DC lines rating, etc.). We also propose a coordination methodology to further enhance AC and DC stabilities.

To perform the simulation studies, the perturbation scenario was chosen to solicit the control of multiple stability aspects simultaneously. A generation loss (G4) in right side of the AC zone 1 was the final choice since it excites inter-area oscillations (POD need), increases angle differences on the boundaries of the AC intertie line (ADC need) and induces an unbalance between production and consumption (FCR need). DC voltage support is needed particularly in case 3 (combination of different controllers without coordination) that will be shown hereby. In this paper, communication between controllers is considered to be well-established in all the cases where ancillary services are implemented.

3.1. Ancillary Services Combination and Case Studies

The strategies to propose ancillary services by an MTDC Grid can be defined as per the targeted objectives: small-signal stability support, rotor angle support and frequency support.

The implementation of these services can be distinguished by their level of communication and their degree of coordination. The coordination degree will be studied in Section 0. Potential use cases are cited below:

- In the basic application, the HVDC system is only used for power dispatching alongside controlling the DC voltage to avoid HVDC grid from collapsing.
- Communication-free cases include controls based on local measurements like for frequency support tested in Section 0. A more detailed study of its interactions with DC voltage support was made in the paper [ref my paper] and its drawbacks were also shown.
- Communication-based cases make usage of WAMS either for rotor angle support [39]–[41] or frequency support too.
- Coordination is useful when multiple controls are implemented to propose better stability enhancement control schemes.

In the following, a comparative study is made between the stability enhancement strategies on the same comprehensive benchmark composed of two AC systems connected through a four-terminal meshed MMC-based MTDC system (Fig. 1). The final aim is to define a coordination strategy between the ancillary services.

For each proposed ancillary service, the corresponding controller was tuned to individually with respect to AC and DC stability performances (oscillation damping, AC line emulation, frequency support with limited interaction with DC voltage control) for a maximal loss of 450 MW (a loss of 12.5% of the total nominal power in the disturbed AC zone) on one side of one of the AC zone 1. For the considered simulation conditions, the implemented control gains are shown in the Table 4. Contingency and parameters of the implemented controls for the study.Table 4. The ADC was designed to at least reduce by 50% the steady-state power deviation in the observed AC tie line (Fig. 5 in next section). The POD was designed to damp the oscillations within 4s after the contingency (Fig. 8 in next section). The FCR was designed to deliver all a converter's nominal active power headroom (1 GW) for a frequency deviation of 0.5 Hz from the nominal value (50 Hz) constrained by the converter's remaining active power headroom.

Table 4. Contingency and parameters of the implemented controls for the study.

Contingency	Parameters of the ADC	Parameter of the POD	Parameter of each FCR droop	Parameter of DC voltage droop
Loss of G4 (450 MW or 12.5% of total nominal power in AC zone 1, at t=1s	K_{ADC} = 1005 MW / τ_{ADC} = 5 s	K_{POD} = 2500 MW / Hz	K_{FCR} = 2000 MW / Hz	$K_{V_{dc}}$ = 8 MW / kV

A comparative study is made between different stability enhancement strategies. Each strategy consists of a combination of the studied controllers. The objective is to propose a coordination strategy between the multiple HVDC ancillary services to enhance global AC stability.

3.2. Comparative study and Problem Exposition

Through the case studies, the need of power coordination appears mostly when all the selected ancillary services coexist. The coordination strategy is proposed in the last case study.

Tests of stability enhancement strategies are the following:

- Case 0 – Reference case w/o suppl. control.

- Case 1 – w/ {POD}, w/o {ADC + FCR}: small-signal stability is only tackled.
- Case 2 – w/ {ADC + POD}, w/o {FCR}: small-signal and rotor angle steady-state stabilities are tackled.
- Case 3 – w/ {ADC + POD + FCR}: small-signal, rotor angle steady-state and frequency stabilities are tackled.
- Case 4 – w/ {ADC + POD + FCR}, w/ coordination: same as case 3 but in an enhanced way.

The selected physical quantities to compare are:

- Measured frequency deviation from nominal value (50 Hz) of each remaining machine in AC zone 1.
- Active power output of each converter.
- Active power flow at one AC tie line in AC zone 1 (line between buses 7 and 8 in the AC zone 1). The observed tie line is mentioned in Fig. 1.
- DC voltage at converter S2.

3.2.1. Case 0 – Reference case w/o suppl. control

After the contingency happens, the frequency of the remaining connected machines decreases as shown in Fig. 6. The frequency Nadir reaches 49.17 Hz while the frequency's steady-state value is 49.73 Hz. Inter-area oscillations appear between {G1, G2} and {G3, G5}. The power oscillations are of almost 150 MW in the observed AC tie line (Fig. 5). The oscillations are damped after the PSSs in AC zone 1 return to their unsaturated working area (like the case shown in Fig. 3.c). In this reference case, the power outputs of the stations remain unchanged because no HVDC service is implemented.

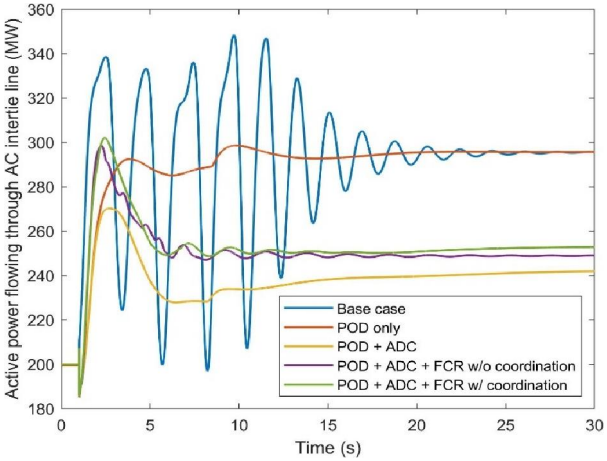

Fig. 5. Active Power flowing through the observed AC tie line in different stability enhancement strategies.

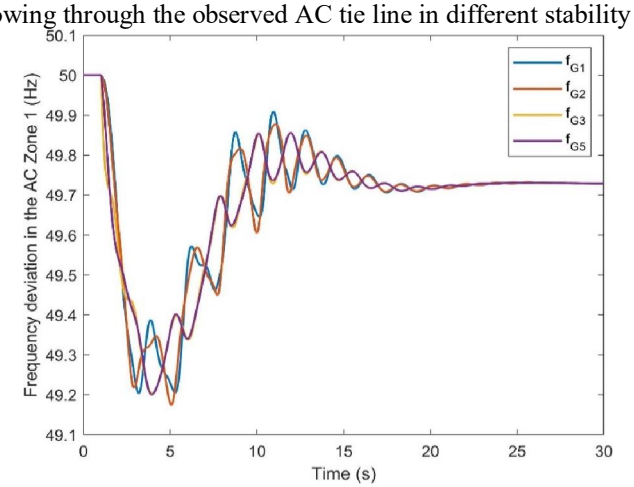

Fig. 6. Frequency deviation from nominal value of the remaining connected generators in AC zone 1 in reference case. The group {G1, G2} oscillates against the group {G3, G5}.

3.2.2. Case 1 – w/ {POD}, w/o {ADC + FCR}

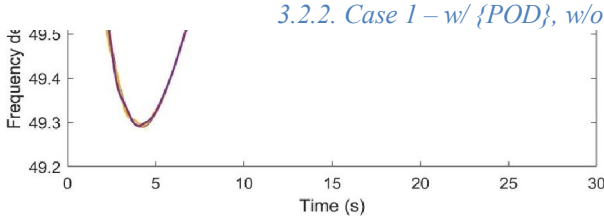

- POD controllers, each one based on the frequency S3 and S4, are added. The Results in Fig. 8 and Fig. 5 g time (4s vs 25s in Case 0). By design, when the inter- ıtputs of the converters come back to initial values (at ly modified during the disturbance (

Fig. 7). Although the small-signal stability was enhanced, the HVDC system can still propose new ancillary services to enhance frequency and rotor angle stabilities.

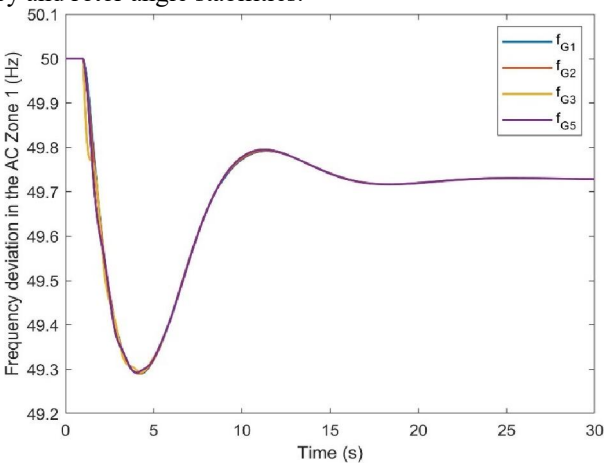

Fig. 7. Active power output of the stations S1, S2, S3 and S4.

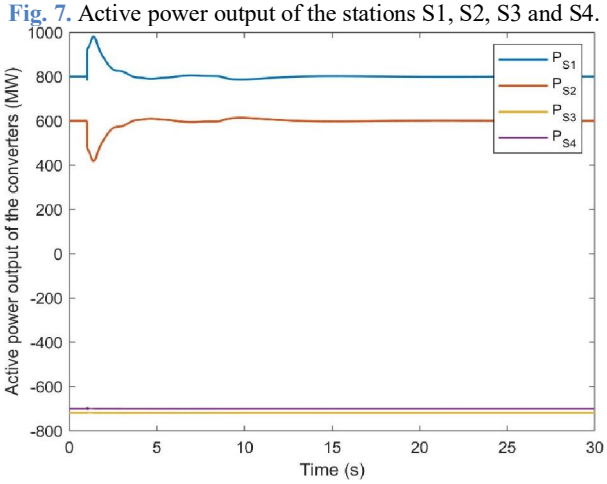

Fig. 8. Frequency deviation from nominal value of the remaining connected generators in AC zone 1 after POD was added.

3.2.3. Case 2 – w/ {ADC + POD}, w/o {FCR}

In the previous case, the active power increase in each of the AC tie lines is relatively high (95 MW per line, 47.5% of the initial value, Fig. 5). Consequently, in Case 2, DC system emulates AC lines thanks to the ADC that uses the measured electric angles at the PCCs.

This ADC control changes the steady-state power output of S1 by +100 MW and S2 for -100 MW (Fig. 10). By transmitting power through the HVDC system, the AC tie lines are less loaded (42 MW per line, 21% of the initial value, Fig. 5) and therefore less sensitive to tripping. The risk of system split in AC zone 1 is also reduced since the rotor angles difference at the boundaries of the observed tie line is decreased by the ADC.

The DC voltage is almost unmodified since the same amount of active power is extracted from one area (left side) of the AC zone 1 and reinjected in the other area (right side) (Fig. 9).

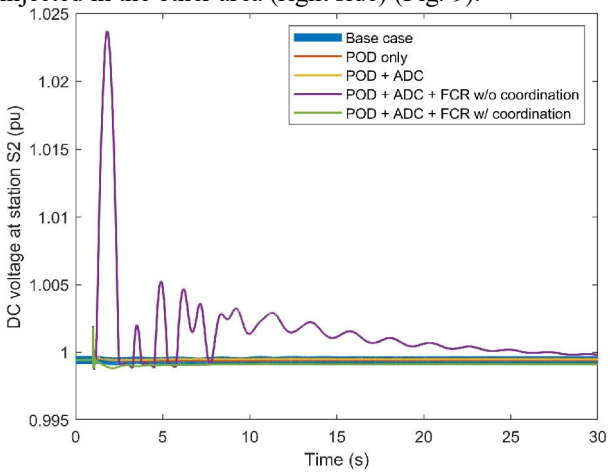

Fig. 9. DC voltage at the DC terminal of station S2 in different stability enhancement strategies.

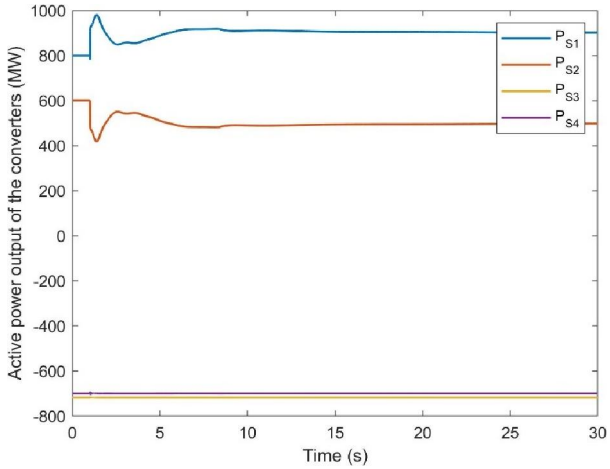

Fig. 10. Active power output of the stations S1, S2, S3 and S4.

3.2.4. Case 3 – w/ {ADC + POD + FCR}

To enhance frequency stability (in this paper, deviation from nominal value at frequency Nadir, and steady-state), FCR control layer was added to the control of MTDC system. The frequency deviations are shown in Fig. 11.

The FCR increases the frequency Nadir to 49.61 Hz which means a reduction of the deviation from the nominal frequency (50 Hz) by 47% compared to the value in Case 0. The steady-state value of the frequency is 49.85 Hz which corresponds to an enhancement by 56% as per the same base case.

Nevertheless, although the FCR helps desaturate the PSS more quickly, the inter-area oscillations between {G1, G2} and {G3, G5} reappear. To explain this phenomenon, the power exchanged by the converters with AC sides are plotted in Fig. 12. During the disturbance, station S2 can effectively extract the necessary amount of power at the PCC to damp the oscillations while, due to the combined action of the FCR, station S1 is only able to inject limited damping power at its PCC. This is due to the limitation of the output of the converters that prevents the area of {G1, G2} from receiving the needed power. Therefore, as shown in Fig. 11, oscillations are less damped – in amplitude and duration – than when small-signal stability was individually enhanced by the POD (Case 1, Fig. 8). Moreover, with POD control, since the station S1 injects in AC system less active power (due to S1's saturation) than station S2 extracts from it, the DC voltage increases slightly in HVDC system (2.4%, Fig. 9).

In conclusion, although the POD and the FCR inject power in the same direction at S1, they interact in an antagonist way during disturbance due to the existing power constraints of the converter station. Their interaction also decreases the DC voltage stability. Therefore, a coordination strategy is needed at least between these two controls to limit or prevent antagonist effects from happening.

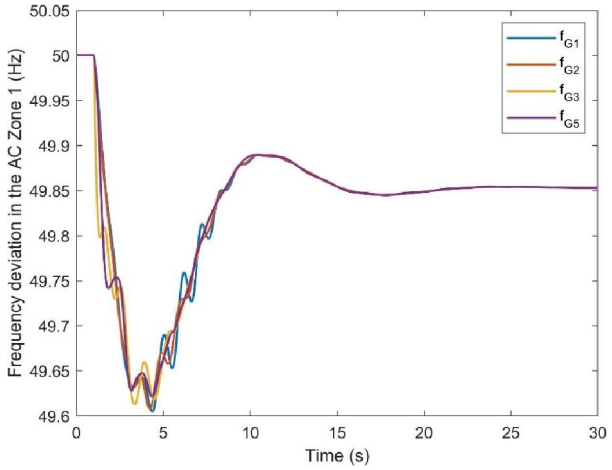

Fig. 11. Frequency deviation from nominal value of the remaining connected generators in AC zone 1 after POD, ADC and FCR were added to the control of the MTDC.

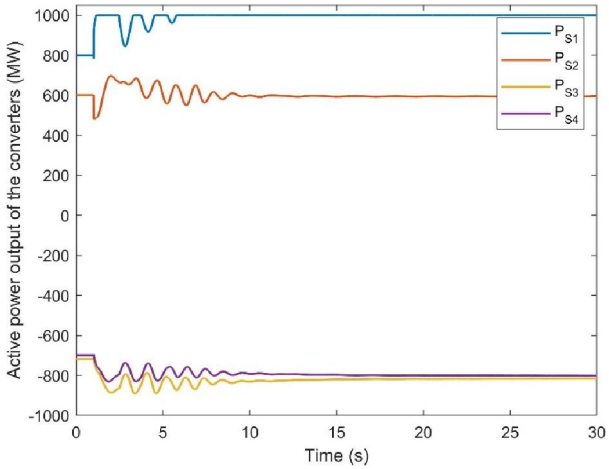

Fig. 12. Active power output of the stations S1, S2, S3 and S4.

3.2.5. Coordination strategy and Case 4 – w/ {ADC + POD + FCR}, w/ coordination

3.2.5.1. Proposed coordination strategy

In the following, a conservative but secure strategy is proposed for the coordination of the different HVDC ancillary services from an AC/DC Power System perspective. In other works, a less conservative strategy is proposed with and without the control coordination strategy developed in this paper. In those yet unpublished works, Particle Swarm Optimization is applied using Python MealPy© library. This metaheuristic optimization layer tested with and without control coordination, enhances stability further by finding optimal combination of control parameters that would minimize an objective function calculated based on weighted key performance indicators of stability. The Dymola©-Python© interface is developed to let Python automatically run the power system models and find best control parameters. Other approaches using Functional Mock-Up Interface (FMI) and Functional Mock-Ups (FMUs) were tested and validated as well for further studies.)

3.2.5.1.1. Headroom fragmentation and allocation

When implemented, each ancillary service sends an active power control reference to the converter which may be able to fulfill it or not depending on its remaining headroom. This means that all the services share the same remaining headroom and, if the tuning of the control parameters (gains and time constants of the filters) is not updated regularly, one or more control(s) will saturate the involved converter, leaving less or no room for other control references. This was the issue in case 3 since control parameters were not changed during simulation.

However, regular retuning of the parameters of POD, ADC and FCR is not common since the parameters of the converters' controllers are usually calibrated depending on the operating conditions of the grid as is the case of Hydro Quebec and RTE [42], [43]. For the sake of research, the solution of parameter retuning was tested for our benchmark and the available results showed enhancement of the mentioned stabilities, but the work presented in this paper aims to propose a solution that avoids regular proportional gain retuning.

The idea in this paper is to propose a solution that guarantees that each control power reference is accomplished without changing the gains and time constants of the controllers too frequently. To do so, the concept of headroom fragmentation was developed. To secure the correct operation of the controllers corresponding to the proposed ancillary services (POD, ADC and FCR in our case), the remaining headroom of the contributing converters was fragmented and allocated to different services before the occurrence of any contingency. This compartmentation within the constrained remaining headroom ensures that no controller dominates another one when the contingency happens. It consequently allows the TSO to decide on how the ancillary services will be allocated by the HVDC system for a given power flow and most credible contingency scenarios.

Practically, for each service, a controller is implemented, and pairs of converters are used to transfer the power sent by the controller's references. To conserve power balance in the MTDC system, the power reference sent to a converter k is sent the same but in opposite direction to the converter j of the pair kj of converters used for a given control. A 'virtual link kj' corresponds to a control (ADC, POD or FCR in our paper) operating in the pair of converters kj where effort is made by converter k. The 'virtual link' is specifically created between these converters to transfer the needed power between them. The mentioned 'headroom per service' of the previous paragraph can be interpreted as virtual link saturation. Paradoxically, to enhance the global stability of an AC/DC system, each of these links should have an upper and lower limit to prevent a given control from dominating the others so that we ensure the correct operation of all controllers.

The mathematical formulation of the previous functioning of control and the mathematical foundation of the proposed headroom allocation concept are presented in the following. For the sake of clarity, only power injection and ancillary services are considered in the control scheme.

For a system composed of a set $\mathcal{N}$ of N AC/DC converters, the following is the active power reference sent to converter k, $\forall k \epsilon \{1, .., N\}$:

$$P^*_{conv_k} = P^0_{conv_k} + \sum_{j=1}^{N} P^*_{ADC,kj} + \sum_{j=1}^{N} P^*_{POD,kj} + \sum_{j=1}^{N} P^*_{FCR,kj} \quad (7)$$

which can be reduced to:

$$P^*_{conv_k} = P^0_{conv_k} + \sum_{j \in \mathcal{S}_k} P^*_{ADC,kj} + \sum_{j \in \mathcal{S}_k} P^*_{POD,kj} + \sum_{j \in \mathcal{A}_k} P^*_{FCR,kj} \quad (8)$$

where:

- $P^0_{conv_k}$ is the active power reference sent by power dispatch (initial power before any contingency)
- $P^*_{ADC,kj}$ is the active power reference sent to converter k by the ADC implemented between converters k and j (check equations
- *P∗ADCkjt=KADC,kj·θjt−θkt (3.a) PADC∗jkt= − PADC∗kjt (3.b)*
- $P^*_{POD,kj}$ is the active power reference sent to converter k by the POD implemented between converters k and j (
- $P^*_{FCR,kj}$ is the active power reference sent to converter k by the FCR implemented between converters k and j (
- $\mathcal{N}$ is the set of AC/DC converter index connected considered in the HVAC/HVDC system.
- $\mathcal{S}_k$ is the set of converter index connected to the same synchronous zone as converter k.
- $\mathcal{S}_k = cardinality(\mathcal{S}_k)$ is the number of elements in $\mathcal{S}_k$. If a converter $j \epsilon \mathcal{S}_k$ does not contribute to the ADC (respectively POD), the corresponding gain $K_{ADC,kj}$ (respectively $K_{POD,kj}$) is set to 0.
- $\mathcal{A}_k$ is the set of converter index connected to a different synchronous zone from converter k.
- $\mathcal{A}_k = cardinality(\mathcal{A}_k)$ is the number of elements in $\mathcal{A}$. If a converter $j \epsilon \mathcal{A}_k$ does not contribute to the FCR, the corresponding gain $K_{FCR,kj}$ is set to 0.

Before headroom fragmentation, the control law of the converter k was constrained as:

$$P^{min}_{conv_k} \leq P^*_{conv_k} \leq P^{max}_{conv_k} \quad (9)$$

where $P^{min}_{conv_k}$ and $P^{max}_{conv_k}$ are respectively the lower and upper rated power of converter k.

$$P^{min}_{conv_k} \leq P^*_{conv_k} \leq P^{max}_{conv_k} \quad (9)$$

gives:

$$P^{min}_{conv_k} - P^0_{conv_k} \leq \sum_{j \in \mathcal{S}_k} P^*_{ADC,kj} + \sum_{j \in \mathcal{S}_k} P^*_{POD,kj} + \sum_{j \in \mathcal{A}_k} P^*_{FCR,kj} \leq P^{max}_{conv_k} - P^0_{conv_k} \quad (10)$$

The headroom $[P^{min}_{conv_k} - P^0_{conv_k}\ ;\ P^{max}_{conv_k} - P^0_{conv_k}]$ is commonly shared between the different ancillary services controllers. This was the case shown in 0 and the results showed degraded global stability as was explained before.

To cope with this issue, headroom fragmentation and allocation per virtual link are proposed as the following equations show. Since ADC and POD act on decoupled timescales, their headrooms can be shared as it will be shown below. Since the FCR may be active during disturbances and at steady-state, its headroom is separated from that of the ADC and POD.

In the following, the power reference sent by a controller to a given pair of converters kj is noted $P^*_{virtual\ link,kj}$ where the 'virtual link' corresponds to 'ADC', 'POD' or 'FCR'. The set of virtual links is noted $\mathcal{V} = \{'ADC','POD','FCR'\}$.

The sum of all possible virtual links $v\epsilon\mathcal{V}$ corresponding to the pair kj with the converters $j\epsilon\mathcal{N}\backslash k$ is noted as $\Delta P^*_{conv_k,tot}$:

$$\Delta P^*_{conv_k,tot} = P^*_{conv_k,tot} - P^0_{conv_k} = \sum_{v\epsilon\mathcal{V}}\sum_{j=1}^{N} P^*_{v,kj} = \sum_{j\in\mathcal{S}_k} P^*_{v,kj} + \sum_{j\in\mathcal{A}_k} P^*_{v,kj} \quad (11)$$

where $P^*_{v,kj}$ corresponds to the power reference sent to station k by the virtual link v that connects it with station j.

To distinguish between power injection and extraction, two headroom zones (above and below $P^0_{conv_k}$) within the total headroom of the considered converter k are separated for fragmentation and allocation. For each virtual link v corresponding to a control ({ADC and/or POD} or FCR) implemented between the converter k and j, the headroom fragmentation is designed as the following:

- Fragmentation of the remaining headroom above $P^0_{conv_k}$:
-
$$\begin{cases} P^{min}_{v,kj} = 0 \le P^*_{v,kj} \le P^{max}_{v,kj} \\ P^{max}_{v,kj} = -P^{min}_{v,jk} \end{cases} \quad (12)$$

  where:
  - $P^*_{v,kj}$ is the power reference sent to converter k by the virtual link v corresponding to a controller ({ADC and/or POD} or FCR) implemented between converters k and j.
  - $P^{max}_{v,kj}$ and $P^{min}_{v,kj}$ are respectively the upper and lower limits (check section 0 for value definition) of the power flowing through the virtual link v for the pair of converters kj considered at station k.
  - $P^{min}_{v,jk}$ is the lower limit considered for the same virtual link v, kj considered at station j.

  This means that the power reference $P^*_{v,kj}$ sent to converter k through the virtual link kj is limited within the range [0; $P^{max}_{v,kj}$] (first part of equation

  $$\begin{cases} P^{min}_{v,kj} = 0 \le P^*_{v,kj} \le P^{max}_{v,kj} \\ P^{max}_{v,kj} = -P^{min}_{v,jk} \end{cases}$$

  (12)) which must be identical but in opposite direction at the level of converter j (second part of equation

  $$\begin{cases} P^{min}_{v,kj} = 0 \le P^*_{v,kj} \le P^{max}_{v,kj} \\ P^{max}_{v,kj} = -P^{min}_{v,jk} \end{cases}$$

  (12)).

- Fragmentation of the remaining headroom below $P^0_{conv_k}$:
-
$$\begin{cases} P^{min}_{v,kj} \le P^*_{v,kj} \le 0 = P^{max}_{v,kj} \\ P^{min}_{v,kj} = -P^{max}_{v,jk} \end{cases} \quad (13)$$

  This means that the power reference $P^*_{v,kj}$ sent to converter k through the virtual link kj is limited within the range [$P^{min}_{virtual\ link,kj}$; 0] (first part of equation

  $$\begin{cases} P^{min}_{v,kj} \le P^*_{v,kj} \le 0 = P^{max}_{v,kj} \\ P^{min}_{v,kj} = -P^{max}_{v,jk} \end{cases}$$

  (13)) which must be identical but in opposite direction at the level of converter j (second part of equation

$$\begin{cases} P_{v,kj}^{min} \leq P_{v,kj}^{*} \leq 0 = P_{v,kj}^{max} \\ P_{v,kj}^{min} = -P_{v,jk}^{max} \end{cases}$$

(13)).

T

W

$$P_{v,kj}^{min} \leq P_{v,kj}^{*} \leq P_{v,kj}^{max} \tag{14}$$

Where $P_{v,kj}^{min} = 0$ if v operates in the headroom above $P_{conv_k}^{0}$, and $P_{v,kj}^{max} = 0$ in the opposite case.

W

$$\begin{cases} \sum_{v\epsilon\mathcal{V}} \sum_{j=1}^{N} P_{v,kj}^{max} = \sum_{v\epsilon\mathcal{V}} \left(\sum_{j\in\mathcal{S}_k} P_{v,kj}^{max} + \sum_{j\in\mathcal{A}_k} P_{v,kj}^{max} \right) = \sum_{v\epsilon\mathcal{V}} \sum_{j\in\mathcal{S}_k} P_{v,kj}^{max} + \sum_{v\epsilon\mathcal{V}} \sum_{j\in\mathcal{A}_k} P_{v,kj}^{max} \\ \sum_{v\epsilon\mathcal{V}} \sum_{j=1}^{N} P_{v,kj}^{min} = \sum_{v\epsilon\mathcal{V}} \left(\sum_{j\in\mathcal{S}_k} P_{v,kj}^{min} + \sum_{j\in\mathcal{A}_k} P_{v,kj}^{min} \right) = \sum_{v\epsilon\mathcal{V}} \sum_{j\in\mathcal{S}_k} P_{v,kj}^{min} + \sum_{v\epsilon\mathcal{V}} \sum_{j\in\mathcal{A}_k} P_{v,kj}^{min} \end{cases} \tag{15}$$

At this stage, all virtual links are constrained by lower and upper limits. However, another condition on the sum

T

$$\begin{cases} \sum_{v\epsilon\mathcal{V}} \sum_{j=1}^{N} P_{v,kj}^{max} \leq P_{conv_k}^{max} - P_{conv_k}^{0} \\ \sum_{v\epsilon\mathcal{V}} \sum_{j=1}^{N} P_{v,kj}^{min} \leq P_{conv_k}^{min} - P_{conv_k}^{0} \end{cases} \tag{16}$$

I

F

M

$$P_{conv_k}^{min} - P_{conv_k}^{0} \leq \sum_{v\epsilon\mathcal{V}} \sum_{j=1}^{N} P_{v,kj}^{min} \leq \Delta P_{conv_k,tot}^{*} \leq \sum_{v\epsilon\mathcal{V}} \sum_{j=1}^{N} P_{v,kj}^{max} \leq P_{conv_k}^{max} - P_{conv_k}^{0} \tag{17}$$

2.5.1.2. Coordination of headroom

The headroom fragmentation and allocation per virtual link presented in the previous paragraph requires coordination which solves the following problem: what exact values should be given for the upper and lower limits of the allocated headroom per service to enhance the global stability of the AC/DC power system compared to the case 3 (0) with common headroom?

Pv, kjmin≤Pv, kj≤Pv, kjmax*

(14), the sum of all headrooms (respectively above and below $P_{conv_k}^{0}$) is given by:

To solve this issue, coordination is realized following these two rules:

- The headroom of {ADC+POD} are defined before the ones of the FCR since AC system split should be avoided in priority to maintain synchronism within the same AC zone. In fact, synchronous AC zones are usually equipped with frequency primary and secondary reserves which are designed for the worst frequency contingency (e.g., loss of 3GW generation within CE synchronous zone AC system [44]). Consequently, after designing headroom for {ADC+POD} services, if the HVDC system can still offer FCR services, the remaining headroom is used for it.
- To calculate the headroom for {ADC+POD}, a heuristic approach is adopted for a given power flow and a given worst case contingency scenario. It is explained in the following. The simulation results which show the required amount for ADC and/or POD per converter are used to implement the upper and lower limits of the virtual links as defined in Section 0. Practically, a tradeoff between the amounts of allocated headroom per controller should be found in order to enhance the global stability of the hybrid AC/DC system. In this paper, the tradeoff is found by sweeping headroom parameters in the simulation environment with headroom values around the actual power references sent by ADC, POD and FCR. An optimization-based approach could be adopted for a better tradeoff.

  The section 0 describes how headroom fragmentation, allocation and coordination was realized for our study case 4 using the benchmark presented in Fig. 1.

3.2.5.2. Case 4 – w/ {ADC + POD + FCR}, w/ coordination

In our case, the headrooms of the stations {S1, S2, S3, S4} are represented in the Fig. 13 (bar plots).

Around initial powerflow value, POD and ADC actions have fixed headrooms. The remaining headroom of each station is allocated for FCR. FCR exists between the "virtual links" S1-S3, S1-S4, S2-S3 and S2-S4: when one converter of a couple extracts power from an AC zone, the other injects same amount in the other synchronous AC zone of the benchmark. The FCR headroom allocation is arbitrarily chosen equal between S1-S3 and S1-S4 from one side, and S2-S3 and S2-S4 from the other side (see blue block in Fig. 13**Erreur ! Source du renvoi introuvable.**). With the two-rules approach described in the section 0, for case 4, the allocated headrooms corresponding to the used power flow and the previously defined contingency scenario are mentioned in **Erreur ! Source du renvoi introuvable.** which is explained below.

Table 5. Coordinated headroom allocation (in solicited zone) per actual virtual link.

Station	Control	Allocated headroom range (MW)
S1	$[POD + ADC]_{12}$	$[0; 125]$
	$FCR_{13} + FCR_{14}$	$[0; 37.5] + [0; 37.5]$
S2	$[POD + ADC]_{21}$	$[0; 125]$
	$FCR_{23} + FCR_{24}$	$[0; 137.5] + [0; 137.5]$
S3	$[POD + ADC]_{34}$	$[0; 125]$
	$FCR_{31} + FCR_{32}$	$[-37.5; 0] + [-137.5; 0]$
S4	$[POD + ADC]_{43}$	$[0; 125]$
	$FCR_{41} + FCR_{42}$	$[-37.5; 0] + [-137.5; 0]$

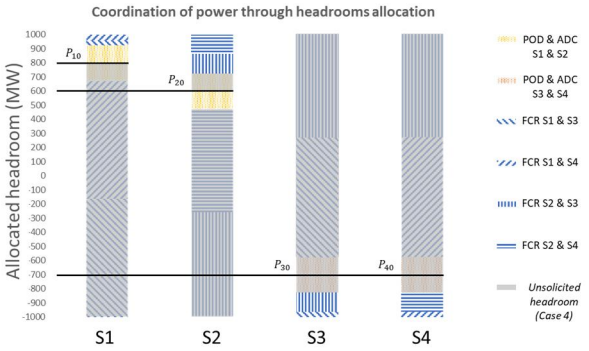

Fig. 13. Coordinated headroom allocation between all stations and per virtual link.

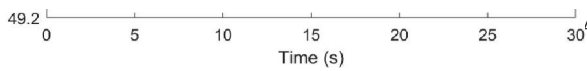

ADC are of ~175 MW and ~100 MW as per Fig. 7 and Fig. 10 respectively. ADC and POD will be combined in a single dedicated headroom since they operate at different time scales. Therefore, the maximal power reference for {ADC + POD} is of 175 MW at S1. Nevertheless, if ±175 MW value is considered for headroom allocation at S1 of virtual link {ADC + POD} between converters S1 and S2, the remaining maximal headrooms for FCR will be 25 MW and 225 MW for S1 and S2 respectively. This amount is not sufficient for frequency stability support. The variation of the headrooms by sweeping their values gives a 'good' tradeoff between rotor angle, small-signal and frequency stability by affecting

±125 MW of maximal headroom for {ADC + POD} at S1 and S2 (and S3 and S4 in our paper) and the remaining for FCR (75 MW at S1, 275 MW at S2, -175 MW at S3 and -175 MW at S4). The approach used is heuristic since it based on simulations (checking if stability aspects are enhanced or not consistently deteriorated with trial and error, starting with virtual link headroom values around the ones sent by the reference of each controller) and it is not yet optimized. A better tradeoff could be found and this is a next step in the elaboration of our active power coordination strategy.

By fixing these headrooms per service, the action of each of them should theoretically be correctly realized and therefore the global stability of the AC/DC system enhanced compared to case 3.

To verify this, the simulation results of case 4 (with coordination) are shown in Fig. 5 (AC line power), Fig. 9 (DC voltage) and Fig. 14 (frequency deviation).

Three observations corresponding to global stability enhancement can be made:

- The frequency oscillations are totally damped after 4 s of the contingency (vs 9 s in case 3, Fig. 11) and their amplitude is reduced (Fig. 11 vs Fig. 14).
- DC voltage is also enhanced since its variation is reduced compared to case 3 (Fig. 9).
- Steady-state AC power flowing through the observed tie-line is only increased by 4 MW compared to case 3 (Fig. 5). This still is an enhancement compared to the cases without ADC.

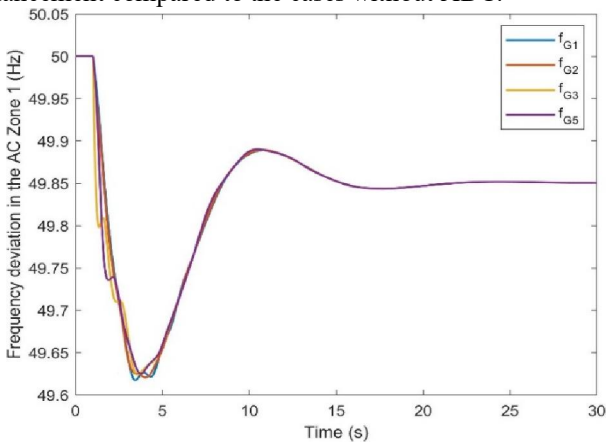

Fig. 14. Frequency deviation from nominal value of the remaining connected generators in AC zone 1 after POD, ADC and FCR were implemented to the control of the MTDC with the proposed coordination strategy.

In conclusion, through the proposed coordination strategy between multiple ancillary services, the global stability of the proposed benchmark was enhanced.

4. Conclusion

This paper focuses on the stability aspects related to rotor angle steady-state, small-signal inter-area oscillations, frequency, and DC voltage. To regulate these aspects, HVDC functionalities were implemented. Respectively, AC line emulation through the regulation of angle difference measured at PCC, power oscillation damping by measuring frequency difference at PCC, frequency containment reserve deployment through distributed power references, and DC voltage droop control. These functionalities (except for DC voltage control) are called ancillary services by HVDC system since they are added to the main functionality of power dispatch affected to this system.

Each ancillary service was tested and validated individually on a proposed comprehensive benchmark power system composed of two separate AC systems (each inspired by 'Kundur' two-area system) connected through a four-terminal MTDC. The functionalities of the HVDC were solicited by different disturbances, each corresponding to a pre-established contingency scenario: AC line trip, load increase and generator trip. The implemented controllers were designed to reduce these potential interactions: POD vs ADC (by tuning the low-pass filter of the ADC) and FCR vs DC voltage droop (by implementing an FCR solution that aims to guarantee power balance in MTDC system).

To evaluate the effectiveness of the implemented controls, different indicators were proposed and used: duration and amplitude of oscillations (for small-signal stability), steady-state deviation of active power flowing through AC tie-line (for rotor angle stability), DC voltage deviation from initial value (during transient), and frequency deviation from nominal value at Nadir and steady-state.

After validation, the ancillary services were combined through different control strategies. A comparative study (using a given initial power flow and generator trip as contingency scenario) showed that the converters' intrinsic active power constraint created control interactions. These should be avoided to deploy the ancillary services more effectively, i.e., to better enhance the AC system's global stability.

A control strategy considering the multiple stability aspects problem was proposed and tested in the current work. It is based on a combination of known control loops (ADC, POD, FCR, DC voltage droop) and involves the converters' headroom fragmentation and allocation. Afterwards, the amount of headroom to allocate per ancillary service was coordinated between the mentioned controllers to further enhance AC/DC hybrid system's stability

compared to the case without coordination of headroom. All this process was mathematically formulated and shown through a picture of the headroom allocation in a separate case study.

Through simulation analysis, stability indicators showed that the proposed coordination strategy enhanced global AC/DC stability. The coordination of headroom was based on a tradeoff between these indicators that the used controllers aim to enhance. The tradeoff was proposed in a heuristic approach but in the future works, an optimization-based approach can be used to find the best headroom coordination. The research focus will be based on developing this optimal approach and on enhancing stability in multiple power flow and contingency scenarios.

Acknowledgements

This work was supported by a grant overseen by the French National Research Agency (ANR) as part of the "Investissements d'Avenir" Program (ANE-ITE-002-01) of the French Government.

References

[1] B. Luscan *et al.*, "A Vision of HVDC Key Role Toward Fault-Tolerant and Stable AC/DC Grids," *IEEE J. Emerg. Sel. Top. Power Electron.*, vol. 9, no. 6, pp. 7471–7485, Dec. 2021, doi: 10.1109/JESTPE.2020.3037016.

[2] L. Meegahapola, S. Bu, and M. Gu, *Hybrid AC/DC Power Grids: Stability and Control Aspects*. in Power Systems. Cham: Springer International Publishing, 2022. doi: 10.1007/978-3-031-06384-8.

[3] Y. Chompoobutrgool and L. Vanfretti, "Identification of Power System Dominant Inter-Area Oscillation Paths," *IEEE Trans. Power Syst.*, vol. 28, no. 3, pp. 2798–2807, Aug. 2013, doi: 10.1109/TPWRS.2012.2227840.

[4] L. Yazdani and M. R. Aghamohammadi, "Damping inter-area oscillation by generation rescheduling based on wide-area measurement information," *Int. J. Electr. Power Energy Syst.*, vol. 67, pp. 138–151, May 2015, doi: 10.1016/j.ijepes.2014.11.018.

[5] Y. Zhang and A. Bose, "Design of Wide-Area Damping Controllers for Inter-area Oscillations," *IEEE Trans. Power Syst.*, vol. 23, no. 3, pp. 1136–1143, Aug. 2008, doi: 10.1109/TPWRS.2008.926718.

[6] A. Sheykhsarraf, M. Abedini, and M. Davarpanah, "A novel method for optimal placement and tuning of the power system stabilizer in the multi-machine system," *Electr. Power Syst. Res.*, vol. 221, p. 109451, Aug. 2023, doi: 10.1016/j.epsr.2023.109451.

[7] W. Gao, R. Fan, R. Huang, Q. Huang, W. Gao, and L. Du, "Augmented random search based inter-area oscillation damping using high voltage DC transmission," *Electr. Power Syst. Res.*, vol. 216, p. 109063, Mar. 2023, doi: 10.1016/j.epsr.2022.109063.

[8] Z. Rafique, H. M. Khalid, S. M. Muyeen, and I. Kamwa, "Bibliographic review on power system oscillations damping: An era of conventional grids and renewable energy integration," *Int. J. Electr. Power Energy Syst.*, vol. 136, p. 107556, Mar. 2022, doi: 10.1016/j.ijepes.2021.107556.

[9] Y. Wen, C. Y. Chung, and X. Ye, "Enhancing Frequency Stability of Asynchronous Grids Interconnected with HVDC Links," *IEEE Trans. Power Syst.*, vol. 33, no. 2, pp. 1800–1810, Mar. 2018, doi: 10.1109/TPWRS.2017.2726444.

[10] A. Bucurenciu, M. Ndreko, M. Popov, and M. A. M. M. Van Der Meijden, "Frequency response using MTDC grids: A comparative study of common methods," in *2015 IEEE Eindhoven PowerTech*, Eindhoven, Netherlands: IEEE, Jun. 2015, pp. 1–6. doi: 10.1109/PTC.2015.7232833.

[11] J. Fradley, R. Preece, and M. Barnes, "VSC-HVDC for Frequency Support (a review)," in *13th IET International Conference on AC and DC Power Transmission (ACDC 2017)*, Manchester, UK: Institution of Engineering and Technology, 2017, p. 62 (6 .)-62 (6 .). doi: 10.1049/cp.2017.0062.

[12] Q. Zhang *et al.*, "Primary Frequency Support Through North American Continental HVDC Interconnections With VSC-MTDC Systems," *IEEE Trans. Power Syst.*, vol. 36, no. 1, pp. 806–817, Jan. 2021, doi: 10.1109/TPWRS.2020.3013638.

[13] B. Silva, C. L. Moreira, L. Seca, Y. Phulpin, and J. A. Pecas Lopes, "Provision of Inertial and Primary Frequency Control Services Using Offshore Multiterminal HVDC Networks," *IEEE Trans. Sustain. Energy*, vol. 3, no. 4, pp. 800–808, Oct. 2012, doi: 10.1109/TSTE.2012.2199774.

[14] K. Shinoda, G. Bakhos, J. C. Gonzalez-Torres, J. Dai, and A. Benchaib, "FCR Provisions by Multi-Terminal HVDC System".

[15] M. Langwasser, G. De Carne, M. Liserre, and M. Biskoping, "Enhanced grid frequency support by means of HVDC-based load control," *Electr. Power Syst. Res.*, vol. 189, p. 106552, Dec. 2020, doi: 10.1016/j.epsr.2020.106552.

[16] R. Eriksson, J. Beerten, M. Ghandhari, and R. Belmans, "Optimizing DC Voltage Droop Settings for AC/DC System Interactions," *IEEE Trans. Power Deliv.*, vol. 29, no. 1, pp. 362–369, Feb. 2014, doi: 10.1109/TPWRD.2013.2264757.

[17] S. Akkari, J. Dai, M. Petit, and X. Guillaud, "Coupling between the frequency droop and the voltage droop of an AC/DC converter in an MTDC system," in *2015 IEEE Eindhoven PowerTech*, Eindhoven,

Netherlands: IEEE, Jun. 2015, pp. 1–6. doi: 10.1109/PTC.2015.7232285.
[18] J. Beerten, R. Eriksson, and D. Van Hertem, "A new approach to HVDC grid voltage control based on generalized state feedback," in *2014 IEEE PES General Meeting | Conference & Exposition*, National Harbor, MD, USA: IEEE, Jul. 2014, pp. 1–5. doi: 10.1109/PESGM.2014.6939418.
[19] A. S. Kumar and B. P. Padhy, "Headroom based Frequency and DC-Voltage Control for Large Disturbances in Multi-Terminal HVDC (MTDC) Grids," in *2022 IEEE International Conference on Power Electronics, Drives and Energy Systems (PEDES)*, Jaipur, India: IEEE, Dec. 2022, pp. 1–6. doi: 10.1109/PEDES56012.2022.10080455.
[20] A. Benchaib, "Advanced Control of AC/DC Power Networks".
[21] E. Prieto-Araujo, A. Egea-Alvarez, S. Fekriasl, and O. Gomis-Bellmunt, "DC Voltage Droop Control Design for Multiterminal HVDC Systems Considering AC and DC Grid Dynamics," *IEEE Trans. Power Deliv.*, vol. 31, no. 2, pp. 575–585, Apr. 2016, doi: 10.1109/TPWRD.2015.2451531.
[22] J. Renedo, L. Sigrist, L. Rouco, and A. Garcia-Cerrada, "Impact on power system transient stability of AC-line-emulation controllers of VSC-HVDC links." arXiv, Apr. 30, 2021. Accessed: Aug. 02, 2023. [Online]. Available: http://arxiv.org/abs/2104.15039
[23] J. C. Gonzalez-Torres, G. Damm, V. Costan, A. Benchaib, and F. Lamnabhi-Lagarrigue, "A Novel Distributed Supplementary Control of Multi-Terminal VSC-HVDC Grids for Rotor Angle Stability Enhancement of AC/DC Systems," *IEEE Trans. Power Syst.*, vol. 36, no. 1, pp. 623–634, Jan. 2021, doi: 10.1109/TPWRS.2020.3030538.
[24] M. Gu, L. Meegahapola, and K. L. Wong, "Review of Rotor Angle Stability in Hybrid AC/DC Power Systems," in *2018 IEEE PES Asia-Pacific Power and Energy Engineering Conference (APPEEC)*, Kota Kinabalu: IEEE, Oct. 2018, pp. 7–12. doi: 10.1109/APPEEC.2018.8566570.
[25] R. Eriksson, "Coordinated Control of Multiterminal DC Grid Power Injections for Improved Rotor-Angle Stability Based on Lyapunov Theory," *IEEE Trans. Power Deliv.*, vol. 29, no. 4, pp. 1789–1797, Aug. 2014, doi: 10.1109/TPWRD.2013.2293198.
[26] J. Renedo, A. Garcia-Cerrada, and L. Rouco, "Active Power Control Strategies for Transient Stability Enhancement of AC/DC Grids With VSC-HVDC Multi-Terminal Systems," *IEEE Trans. Power Syst.*, vol. 31, no. 6, pp. 4595–4604, Nov. 2016, doi: 10.1109/TPWRS.2016.2517215.
[27] "HVDC links in system operations.pdf." ENTSOE, Dec. 02, 2019. [Online]. Available: https://eepublicdownloads.entsoe.eu/clean-documents/SOC%20documents/20191203_HVDC%20links%20in%20system%20operations.pdf
[28] M. De Castro *et al.*, "Version [OpenIPSL 2.0.0] - [iTesla Power Systems Library (iPSL): A Modelica library for phasor time-domain simulations]," *SoftwareX*, vol. 21, p. 101277, Feb. 2023, doi: 10.1016/j.softx.2022.101277.
[29] S. Boersma, X. Bombois, L. Vanfretti, J.-C. Gonzalez-Torres, and A. Benchaib, "Probing signal design for enhanced damping estimation in power networks," *Int. J. Electr. Power Energy Syst.*, vol. 129, p. 106640, Jul. 2021, doi: 10.1016/j.ijepes.2020.106640.
[30] J. C. Gonzalez-Torres, R. Mourouvin, K. Shinoda, A. Zama, and A. Benchaib, "A simplified approach to model grid-forming controlled MMCs in power system stability studies," in *2021 IEEE PES Innovative Smart Grid Technologies Europe (ISGT Europe)*, Espoo, Finland: IEEE, Oct. 2021, pp. 01–06. doi: 10.1109/ISGTEurope52324.2021.9640024.
[31] R. Mourouvin, J. C. Gonzalez-Torres, J. Dai, A. Benchaib, D. Georges, and S. Bacha, "Understanding the role of VSC control strategies in the limits of power electronics integration in AC grids using modal analysis," *Electr. Power Syst. Res.*, vol. 192, p. 106930, Mar. 2021, doi: 10.1016/j.epsr.2020.106930.
[32] "GridCal tool for powerflow calculation." [Online]. Available: https://github.com/SanPen/GridCal
[33] J. C. Gonzalez-Torres, V. Costan, G. Damm, A. Benchaib, F. Lamnabhi-Lagarrigue, and B. Luscan, "Method for Controlling an Electrical Transmission Network," US 2022/0360089 A1, Nov. 10, 2022 [Online]. Available: https://patents.google.com/patent/US20220360089A1/en
[34] P. Kundur, *Power System Stability And Control*. McGraw-Hill, Inc, 1994.
[35] N. R. Chaudhuri, R. Majumder, and B. Chaudhuri, "System Frequency Support Through Multi-Terminal DC (MTDC) Grids," *IEEE Trans. Power Syst.*, vol. 28, no. 1, pp. 347–356, Feb. 2013, doi: 10.1109/TPWRS.2012.2196805.
[36] G. Bakhos, K. SHINODA, J. C. Gonzalez-Torres, A. Benchaib, L. Vanfretti, and S. Bacha, "Aspects of stability issues of HVAC/HVDC coupled grids".
[37] S. Akkari, M. Petit, J. Dai, and X. Guillaud, "Interaction between the Voltage-Droop and the Frequency-Droop Control for Multi-Terminal HVDC Systems".
[38] J. Renedo, L. Rouco, A. Garcia-Cerrada, and L. Sigrist, "Coordinated control in multi-terminal VSC-HVDC systems to improve transient stability: Impact on electromechanical-oscillation damping." arXiv, Jul. 29, 2022. Accessed: Aug. 04, 2023. [Online]. Available: http://arxiv.org/abs/2208.00083
[39] Y. Chompoobutrgool and L. Vanfretti, "Using PMU signals from dominant paths in power system wide-

area damping control," *Sustain. Energy Grids Netw.*, vol. 4, pp. 16–28, Dec. 2015, doi: 10.1016/j.segan.2015.09.001.

[40] K. Uhlen, L. Vanfretti, M. M. De Oliveira, V. H. Aarstrand, and J. O. Gjerde, "Wide-Area Power Oscillation Damper implementation and testing in the Norwegian transmission network," in *2012 IEEE Power and Energy Society General Meeting*, San Diego, CA: IEEE, Jul. 2012, pp. 1–7. doi: 10.1109/PESGM.2012.6344837.

[41] L. Díez-Maroto, L. Vanfretti, M. S. Almas, G. M. Jónsdóttir, and L. Rouco, "A WACS exploiting generator Excitation Boosters for power system transient stability enhancement," *Electr. Power Syst. Res.*, vol. 148, pp. 245–253, Jul. 2017, doi: 10.1016/j.epsr.2017.03.019.

[42] F. Guay, P.-A. Chiasson, N. Verville, S. Tremblay, and P. Askvid, "New Hydro-Québec Real-Time Simulation Interface for HVDC Commissioning Studies".

[43] Y. Vernay, A. D. D'Aubigny, Z. Benalla, and S. Dennetière, "New HVDC LCC replica platform to improve the study and maintenance of the IFA2000 link".

[44] P. Bertolini and M. Emilie, "Documentation Technique de Référence Article 4.1".